DUJASE Vol. 7 (2) 31-38, 2022 (July) *https://doi.org/10.3329/dujase.v7i2.65092*

Robust Signal Denoising Techniques for Highly Accurate and Spatial Resolution Preserved Brillouin Optical Time Domain Analysis Sensors

Abul Kalam Azad

Department of Electrical and Electronic Engineering, University of Dhaka, Dhaka-1000, Bangladesh

E-mail: azad@du.ac.bd

Received on 03 July 2022, Accepted for publication on 09 December 2022

ABSTRACT

The diminution of measurement uncertainty to an acceptable level and the preservation of experimental spatial resolution are highly desirable in many real-world applications of Brillouin optical time domain analysis (BOTDA) sensors. In practical applications of such sensors, the measurement uncertainty essentially relies upon the signal-to-noise ratio (SNR) of the experimental Brillouin gain spectra (BGSs) obtained throughout the sensing fiber. The improvement of such SNR using improper signal denoising techniques alters the experimental spatial resolution of the BOTDA sensors. In this paper, the use of non-local means filter (NLMF) and anisotropic diffusion filter (ADF) is experimentally demonstrated to enhance the uncertainty in the measurement of temperature using BOTDA sensors. For this purpose, the BGSs along a 41 km fiber are collected by averaging several numbers of BOTDA-traces from BOTDA hardware setup. Such BGSs are first denoised by employing NLMF and ADF to improve the measurement SNR. The Brillouin frequency shifts (BFSs) of denoised BGSs are then extracted via curve fitting technique (CFT). The BFS distribution is finally mapped to temperature distribution depending on the known BFS-temperature relationship of the sensing fiber. The robustness of the used filters is analyzed rigorously in terms of SNRs of BGSs, uncertainty in temperature extraction, spatial resolution and runtime in signal processing. The results indicate that the utilization of NLMF and ADF can enhance the SNRs of BGSs up to the maximum of 15.64 dB and 13.53 dB, respectively. Consequently, the uncertainties in the temperature extraction can be reduced up to the maximum of 52.63% and 57.31% for using NLMF and ADF, respectively. Moreover, both NLMF and ADF can preserve the experimental spatial resolution of the BOTDA sensors and include insignificant runtime to CFT. Thus, NLMF and ADF can be considered as robust signal denoising techniques for highly accurate and spatial resolution preserved BOTDA sensors.

Keywords: Distributed optical fiber sensors, Non-local means filter, Anisotropic diffusion filter, Lorentzian function, Least-squares curve fitting.

1. Introduction

Distributed optical fiber sensors (DOFS) offer truly distributed measurement of diverse physical quantity (e.g., temperature, pressure, vibration and strain) along a single span of optical fiber [1 - 4]. The research activities in the recent years manifest the rapid progress of various DOFS technologies. In particular, BOTDA sensors employing stimulated Brillouin scattering (SBS) phenomenon gain immense scholarly interest as it provides long-distant temperature measurement with acceptable uncertainty and spatial resolution [5 - 8]. In a conventional BOTDA sensor [5, 9], the sensing signals within a frequency range are obtained along the fiber in the form of BOTDA-traces. These traces are then combined to obtain Brillouin gain spectra (BGSs) throughout the length of the sensing fiber. The peak frequency of the local BGS is termed as Brillouin frequency shift (BFS) in the literature as it shifts linearly with local temperature enclosing the fiber. Consequently, several thousands of BGSs are obtained throughout the length of the fiber for the determination of distributed temperature using a BOTDA experimental setup. These BGSs are processed using widely-used curve fitting technique (CFT) to extract BFS distribution. The BFS distribution is then converted to obtain the temperature distribution. The experimental BGSs obtained from BOTDA sensors are noisy, especially at the end of a several tens of kilometers long fiber. For this reason, the extracted temperature distribution fluctuates around its actual distribution and introduces uncertainty in the measurement of temperature.

The uncertainty in the measurement of temperature using BOTDA sensors directly relies upon the SNRs of the acquired BGSs [10, 11]. Such uncertainty can be unacceptable for many real-world applications where a long sensing fiber is used in the BOTDA setup. To overcome this limitation, the widely-used technique is to acquire a large number traces from the BOTDA setup [10, 12]. The average operation is then performed on these traces to attain a single trace at an individual selected frequency along the fiber so that the SNRs of BGSs can be improved to an acceptable level. In practical applications, several hundreds of such averaged traces are required to form the BGSs distribution along the fiber. The number of traces averaged (T) during the acquisition of BOTDA traces prolongs the acquisition time of BGSs from BOTDA experiment depending on T and fiber length [5, 12]. To reduce the acquisition time of BGSs with desirable SNR, several alternative techniques using modified BOTDA setups have been studied recently. For instance, optical pulse coding [13, 14], distributed Raman amplification [7, 15], and combination of pulse coding and Raman amplification [16, 17] have been integrated with conventional BOTDA sensors to acquire BGSs with improved SNR. These modified BOTDA experimental setups are complex as well as expensive as compared to conventional BOTDA setup. To avoid the use of such complex and expensive setups, small T is utilized to obtain the noisy BGSs from the conventional BOTDA setup. These noisy BGSs are then denoised by using suitable signal denoising techniques. To do so, different BGSs denoising

techniques such as wavelet transform [18 - 20], adaptive Wiener filtering [21], anisotropic diffusion [22, 23], block matching algorithm [24], and non-local means filtering [18, 25] are reported recently in the literature. However, the consequences of using these denoising techniques on the SNRs of the BGSs, uncertainty in temperature extraction, spatial resolution of the sensors and time required to denoise the BGSs are not investigated meticulously with sufficient experimental results and analysis.

In this experimental study, the use of non-local means filter (NLMF) and anisotropic diffusion filter (ADF) is demonstrated for denoising BGSs obtained from BOTDA experimental setup throughout a 41 km long fiber. The distributions of temperature are extracted from the noisy experimental BGSs as well as from the BGSs obtained after applying NLMF and ADF. The performances of using NLMF and ADF are analyzed for the BGSs obtained with different numbers of traces averaged (T) in the acquisition process. The effects of applying these denoising techniques on the improvement of SNRs of BGSs, uncertainty in the extraction of temperature distributions, spatial resolution and runtime to extract temperature distributions are also analyzed rigorously with adequate experimental results.

2. Hardware Setup of BOTDA Sensor

The conventional hardware setup of BOTDA sensor [5, 9] used for the collection of experimental BGSs is presented in Fig. 1. In the setup, the laser used is tuned at 1550 nm for supplying continuous light wave through the coupler. The coupler splits the wave to deliver light wave through two arms in the setup. The polarization state of continuous light wave launched through two arms is controlled by using two polarization controllers PC1 and PC2. Two electro-optic modulators EOM1 and EOM2 are used in the setup to produce pump pulse and double-sideband suppressed-carrier (DSB-SC) probe wave for the upper and lower arms, respectively. To do so, the EOM1 in the upper arm utilizes a pump pulse generator (PPG) and the EOM2 in the lower arm employs a radio frequency generator (RFG). The power level of the peaks of pump pulses in the upper arm is then amplified to the suitable level by utilizing an erbium-doped fiber amplifier (EDFA). Such amplification process adds amplified spontaneous emission (ASE) noise and the pump pulses get contaminated. To filter out this ASE noise from the upper arm, a band-pass filter (BPF) is utilized. The polarization scrambler (PS) is employed in the upper arm for the minimization of polarization reliant fading of Brillouin gain. Finally, the optical circulator (OC1) directs the pump wave from port 1 to port 2 to be propagated toward the nearest side of the sensing fiber. The power level of the DSB-SC probe wave at the output of the EOM2 in the lower arm is regulated by employing the variable optical attenuator (VOA). Such probe wave is then forward-directed via the optical isolator to be launched toward the furthest side of the sensing fiber.

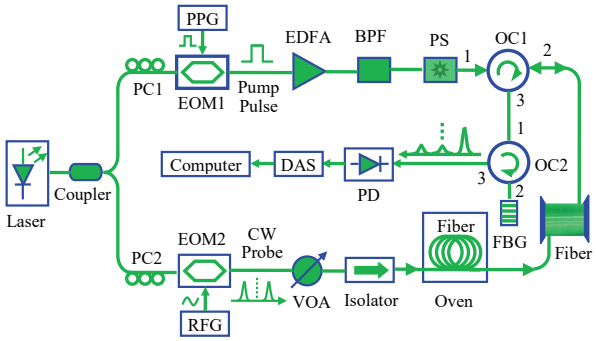

Fig. 1. The hardware setup of conventional BOTDA sensor.

In the hardware setup presented in Fig. 1, the pump and probe waves counter-propagate through the fiber and interact by means of the SBS mechanism. A part of the power is thus delivered from the pump wave to amplify the DSB-SC probe wave. Then, this amplified probe wave is propagated through OC1 from port 2 to port 3. The same wave also propagates through OC2 from port 1 to port 2. The fiber Bragg grating (FBG) filter employed in the hardware arrangement then selects the desired low-frequency sideband to pass from port 2 to port 3 of OC2. Such sideband is then photo-detected and the data acquisition system connected to the output of photo-detector acquires the BOTDA traces adopting a particular number of traces averaged (T) in the acquisition process to form the distribution of BGS along the fiber. These BGSs are stored in the computer and processed for the determination of temperature distribution.

3. Denoising of Experimental BGSs

In recent years, NLMF and ADF have found widespread applications in denoising images [26 - 29] due to their distinct capabilities of removing noise to the greatest extent while preserving edges and details of the image. Consequently, both of these two filters exhibit the capabilities to enhance the SNRs of the noisy BGSs significantly which, in turn reduce the uncertainty in the process of temperature extraction. Moreover, the edge preserving features of these two filters also help to maintain the experimental spatial resolution of the BOTDA sensors. To take the full advantages of these two distinct capabilities, the noisy experimental BGSs obtained from BOTDA sensor depicted in Fig. 1 are collectively treated as an image. Such image comprising numerous BGSs is then denoised by utilizing NLMF and ADF.

3.1 Non-Local Means Filter (NLMF)

The NLMF successfully makes use of the resemblance of neighborhood pixels in an image for reducing noise. The working principle of the filter is based on the fact that there are pixels in the image that contain redundant information and each mini block of pixels in an image have large number of replicas in the image itself. The original image is also supposed to be contaminated by independent and identically distributed Gaussian noise having zero mean and known variance (σ). The typical NLMF utilizes the weighted average

of the intensities of all the pixels in the image to approximate the intensity of a given pixel. These weights are calculated in proportion to the resemblance among the local neighborhood of the pixel to be denoised and that of the local neighborhood of surrounding pixels. In a low-complexity implementation of NLMF, the process of computing weighted average includes a search window S_p of a limited number of pixels neighboring the pixel p.

In NLMF, the denoised intensity $d(p)$ of a pixel p for a noisy image $b(p)$ is determined by [26, 27]

$$d(p) = \hat{b}_{NLM}(p) = \sum_{q \in S_p} w(p,q) b(q) \tag{1}$$

where S_p is a SxS search window centered on pixel p. The weight $w(p,q)$ appraises the resemblance among the intensities of CxC comparison windows $b(N_p)$ and $b(N_q)$ centered on pixels p and q, respectively inside the search window S_p [26]. The resemblance among pixels p and q is evaluated by means of a declining function of the weighted Euclidean distance [27] given by

$$r(p,q) = \left\| b(N_p) - b(N_q) \right\|_{2,\sigma}^2 \tag{2}$$

where, σ is the standard deviation of the Gaussian kernel and its value is greater than zero. The weights in Eq. (1) are then computed [26, 27] by

$$w(p,q) = \frac{1}{z(p)} e^{-\frac{r(p,q)}{h^2}}. \tag{3}$$

In Eq.(3), h regulates the degree of smoothing in using NLMF and $z(p)$ is the normalization constant to ensure that $0 \le w(p,q) \le 1$ and $\sum_q w(p,q) = 1$.

The smoothing parameter (h) in NLMF is a positive number that is estimated to be the standard deviation of noise in the input image comprising noisy experimental BGSs. For the estimation of such standard deviation, the input image is convolved with a 3×3 filter as suggested in Ref [30]. A larger value of h performs more denoising in the image that may cause over-smoothing in the regions containing edges. On the contrary, a small value of h can efficiently preserve edges but can result grainy effect in the denoised image [27, 31]. The other two important parameters involved in the implementation of NLMF are the sizes of search window (S) and comparison window (C). The size of the search window is an odd-valued positive integer that can maximally be equal to the size of the image. A too large value of S may include superfluous and irrelevant pixels to deteriorate the denoising performance of NLMF. The computational cost for implementing NLMF also increases for larger S. On the other hand, a too small value of S selects few numbers of pixels that also affects the performance of the filter [31]. The size of the comparison window (C) is also an odd-valued positive integer that can utmost be equal to the size of S. A too large value of C makes the image too blurred. In effect, the edges in the image cannot be preserved. However, a reasonably small value of C is required for NLMF to perform desired denoising of the input image. Within this scope, the important parameters used in this study for the implementation of NLMF are listed in Table 1.

Table 1: The design parameters of NLMF

Smoothing parameter (h)	Standard deviation of noise
Search window size (S)	21
Comparison window size (C)	5

3.2 Anisotropic Diffusion Filter (ADF)

The basic principle of ADF is governed by the P-M model [28] suggested by Perona and Malik as given by

$$\frac{\partial I(p,q,t)}{\partial t} = div\left[f\left(\left\| \nabla I(p,q,t) \right\| \right) \nabla I(p,q,t) \right]. \tag{4}$$

In Eq. (4), $I(p,q,t)$ is the version of the original image $I(p,q,0)$ at instant t, $\nabla I(p,q,t)$ is the gradient of $I(p,q,t)$ and $f(\bullet)$ is called the conductance function. The function $f(\bullet)$ is chosen in such a way that the maximum diffusion within the uniform regions occurs if $\lim_{x\to 0} f(x) = 1$. On the contrary, the diffusion stops across edges if $\lim_{x\to\infty} f(x) = 0$. To accomplish this, Perona and Malik suggested two functions [28, 29] as given by

$$f_1(x) = \exp\left[-\left(\frac{x}{\kappa} \right)^2 \right] \text{ and} \tag{5}$$

$$f_2(x) = \frac{1}{1 + \left(\frac{x}{\kappa} \right)^2} \tag{6}$$

where κ is termed as the gradient magnitude threshold parameter. This threshold parameter adjusts the diffusion rate depending on the image gradients due to noise and that due to edges. In discrete form, the P-M model yields [29]

$$I_{t+1}(s) = I_t(s) + \frac{\lambda}{|\eta_s|} \sum_{m \in \eta_s} f_k\left(\left| \nabla I_{s,m} \right| \right) \nabla I_{s,m} \tag{7}$$

where I is a discrete image, s is the pixel position in I, t is the time instant and $f\kappa(\bullet)$ is the conductance function at κ. The constant $\lambda \in (0, 1]$ in Eq. (7) controls the rate of diffusion and η_s constitutes the 4-pixel spatial neighborhood of s. This means the fact that $\eta_s = \{N, S, E, W\}$, in which N, S, E and W respectively indicate north, south, east and west neighbors of s. Therefore, η_s is equal to 4 anywhere in I excluding its borders. The operator ∇ in Eq. (7) now denotes a scalar [29], which is defined as

$$\nabla I_{s,m} = I_t(m) - I_t(s) \tag{8}$$

where $m \in \eta_s = \{N, S, E, W\}$. At each iteration of the P-M model, the gradient value in the four directions around the center point is calculated, and the gray level of the original center point is restored by the calculated gradient value.

The implementation of ADF with proper design parameters has good capability in denoising image while preserving the edges. The choice of a suitable conduction function plays important role on the performance of ADF. The conduction function f_1 given by Eq. (5) provides better performance for high-contrast edges compared to low-contrast edges [28, 29]. However, the conduction function f_2 defined by Eq. (6) declines very slowly to zero so as to provide efficient smoothing as well as preserving edges in the image effectively [29]. The gradient threshold (κ) controls the operation of f_κ in Eq. (7) by comparing the gradient values for original edges or noise. A high value of κ performs more smoothing on image. In this study, the value of κ is selected to be 0.1 which is 10% of the dynamic range of the image comprising normalized BGSs having maximum relative amplitude of 1. The spatial neighborhood, also called connectivity, of s in Eq. (7) is selected to be 4, i.e., $\eta_s = \{N, S, E, W\}$. For the effective denoising of image comprising BGSs and to preserve the edges in such image, the filter parameters used in the implementation of ADF in this study are specified in Table 2.

Table 2: The design parameters of ADF

Conduction function (f_κ)	Quadratic [Eq.(6)]
Gradient threshold (κ)	0.1 (10% of dynamic range)
Connectivity (η_s)	4 nearest neighbors

4. Extraction of Temperature Distributions

In this study, the experimental BGSs collected by means of the BOTDA hardware setup shown in Fig. 1 are first denoised by using NLMF and ADF. Then, curve fitting technique (CFT) is applied on the experimental as well as denoised BGSs to extract the distributions of BFS. In CFT, each local BGS is modeled by Lorentzian function [5, 32] given by

$$g(\upsilon) = \frac{g_B}{1 + 4\left[(\upsilon - \upsilon_B)/(\Delta\upsilon_B)\right]^2}. \quad (9)$$

In Eq. (9), υ_B denotes the BFS, g_B denotes the amplitude at BFS and $\Delta\upsilon_B$ denotes the full-width at half-maximum of each BGS. In CFT, nonlinear least-squares curve fitting technique is utilized for fitting each local BGS onto the Lorentzian function. In such technique, the model parameters (i.e., υ_B, g_B and $\Delta\upsilon_B$) of Eq. (9) are updated iteratively to find the best fit for a local BGS [5, 21]. The updated υ_B corresponds to the BFS value for the local BGS. The distribution of BFS obtained after fitting all the BGSs along the fiber are finally mapped to find the temperature distribution by applying the BFS-temperature relationship of the sensing fiber. For the sensing fiber used in this study, the BFS follows a linear variation with temperature having the slope of ~0.929 MHz/°C and the BFS of ~10.829 GHz at 25°C [32].

5. Results and Discussion

In this experimental study, a 41 km single span of sensing fiber is utilized in the hardware setup of BOTDA sensor presented in Fig. 1. A fiber section of ~50 m from the very last end of the used single fiber span is heated inside a constant temperature oven at 45 °C to demonstrate the performance of this BOTDA sensor. The remaining part (i.e., first 40.95 km) of this single fiber span is retained external to the oven at room-temperature of ~21 °C. The BGSs along the entire fiber span are obtained for the frequency ranging from 10.75 GHz to 10.95 GHz at a frequency interval of 1 MHz. Such BGSs are collected by employing pump pulses having 40 ns duration to attain experimental spatial resolution of 4 m.

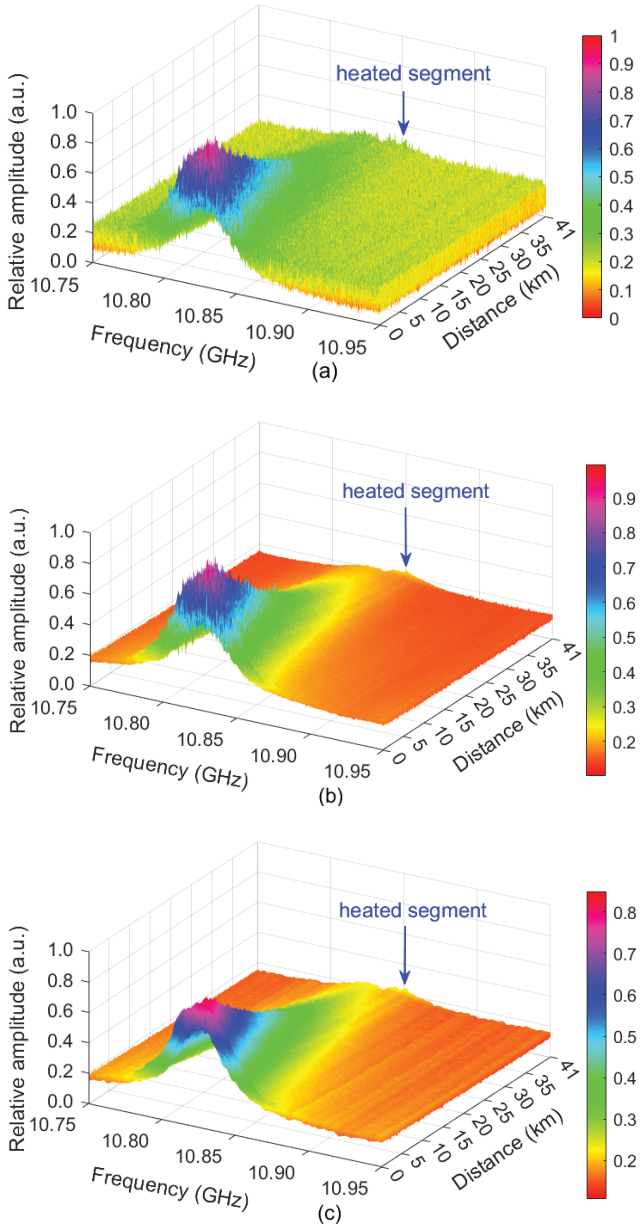

Fig. 2. Distributions of (a) experimental BGSs; and denoised BGSs obtained after applying (b) NLMF and (c) ADF on the experimental BGSs along the 41 km fiber in which the furthest ~50 m fiber section is heated inside the oven.

The BOTDA-traces used to reconstruct the BGSs along the fiber are collected by adopting sampling rate of 125 Mega-symbols/second to fix the BGS spacing of 0.8 m along the fiber. To collect each BOTDA-trace at each frequency, six different numbers of traces of T = 10, 50, 125, 250, 500 and 1000 are averaged to demonstrate the performances of the BOTDA sensor under various noise levels in experimental BGSs. For instance, the experimental BGSs along the 41 km span of fiber collected by averaging 10 traces (i.e., T = 10) is shown in Fig. 2(a). The noisy BGSs collected from BOTDA experiment are then denoised by applying NLMF and ADF separately to reduce the noise-level in the BGSs. The distributions of denoised BGSs obtained after applying NLMF and ADF on experimental noisy BGSs shown in Fig. 2(a) are also presented in Fig. 2(b) and Fig. 2(c), respectively.

It is observed in Fig. 2 that the levels of noise in the denoised BGSs attained after utilizing NLMF and ADF are much lower than that in the experimental BGSs. Consequently, such filters help to improve SNRs of the BGSs. To have a closer look on some particular BGSs at different locations along the fiber in Fig. 2, four experimental noisy BGSs at 10 km, 20 km 30 km and 40.98 km along the 41 km fiber and their corresponding denoised BGSs are plotted in Fig. 3.

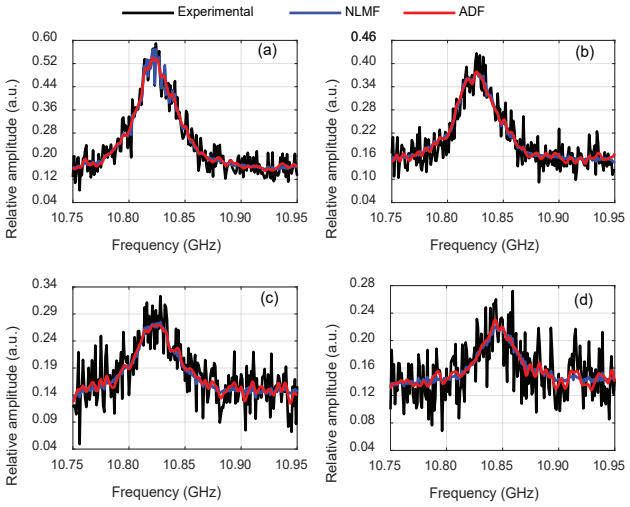

Fig. 3. The experimental and denoised BGSs at locations of (a) 10 km, (b) 20 km, (c) 30 km, and (d) 40.98 km along the 41 km fiber.

The results in Fig. 3 exhibit that the fluctuation of the relative amplitudes of the experimental noisy BGSs increases reasonably with the distance along the fiber due to the accumulation process of noise. It is also found in Fig. 3 that the peak amplitude of the noisy BGSs also decreases remarkably with distance along the fiber due to fiber attenuation. However, it is clearly noticed in Fig. 3 that the use of both NLMF and ADF significantly help to provide low level of noise (i.e., improved SNR) in the BGSs.

To quantify the denoising performances of NLMF and ADF, the SNRs of the experimental noisy BGSs and that of the deoised BGSs obtained after applying these two filters on the experimental BGSs are calculated. In this calculation, the SNRs of the BGSs within the length of the last 50 m fiber section (i.e. worst SNR) heated at constant temperature is considered. Each experimental BGS as well as denoised BGS is then fitted separately with the Lorentzian function given in Eq. (9) and the SNR of a particular BGS is computed as the ratio of peak amplitude of the fitted BGS to the standard deviation of residuals. The SNR at a particular number of traces averaged (T) is finally calculated as the average of the SNRs of all BGSs within the last 50 m fiber section heated inside the oven. The variation of SNR of such experimental and denoised BGSs with T is plotted in Fig. 4.

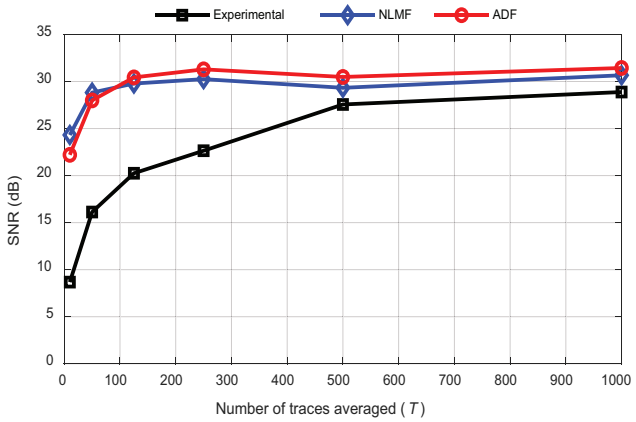

Fig. 4. The SNRs of experimental and denoised BGSs along the furthest 50 m section of the 41 km fiber.

It is easily observed in Fig. 4 that both NLMF and ADF provide significant improvement of SNR for each of the six different numbers of traces averaged in this study. For example, the SNR for the experimental BGSs at T = 10 is ~8.68 dB which has been improved to ~24.32 dB (by ~15.64 dB) and ~22.21 dB (by ~13.53 dB) for using NLMF and ADF, respectively. The SNR improvements at other T for using these two filters are also good. The results in Fig. 4 signify that both NLMF and ADF serve as robust signal denoising techniques for providing higher SNR irrespective of T adopted in this study. It should be noted that the enhancement of SNR for using NLMF and ADF on the experimental BGSs at higher T is lower as the SNRs of the experimental BGSs at higher T are already much higher.

Next, the experimental BGSs along the entire fiber span collected at six different T are denoised separately by applying NLMF and ADF. Then, the process described in section 4 is applied to find the temperature distributions for six different T. For instance, the distribution of temperature along the entire fiber span for the experimental BGSs collected at T = 10 and that for the corresponding denoised BGSs are shown in Fig. 5.

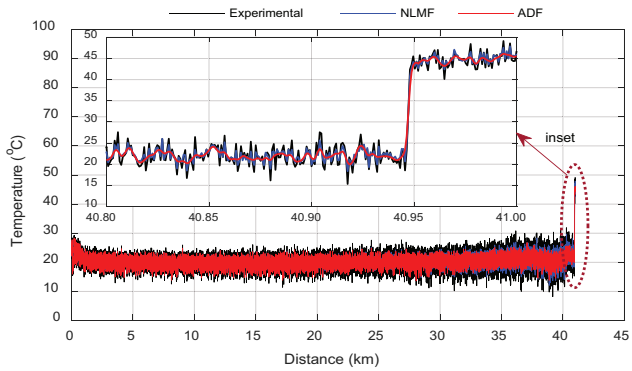

Fig. 5. Distributions of temperature along the 41 km fiber span where the last ~50 m fiber section is heated at 45 °C. Inset shows the distributions of temperature along the furthest 200 m fiber section.

It is observed in Fig. 5 that both NLMF and ADF can be applied to determine the temperature distributions throughout the entire fiber span accurately. The temperature distributions in Fig. 5 also manifest much smaller temperature fluctuations for using these two filters as compared to that for the experimental BGSs. Consequently, the use of both NLMF and ADF helps to reduce the uncertainty of BOTDA sensors in extracting temperature distributions.

The uncertainty in extracting distributions of temperature from the experimental and denoised BGSs are also computed and analyzed in this study. For this, the uncertainty is computed for the last 50 m fiber section heated at 45 °C, where the SNR of the experimental BGSs are the worst. The uncertainty for this fiber section is computed as the standard deviation of the extracted temperatures. The uncertainties calculated for the experimental BGSs and their corresponding denoised BGSs obtained after applying NLMF and ADF are shown in Fig. 6.

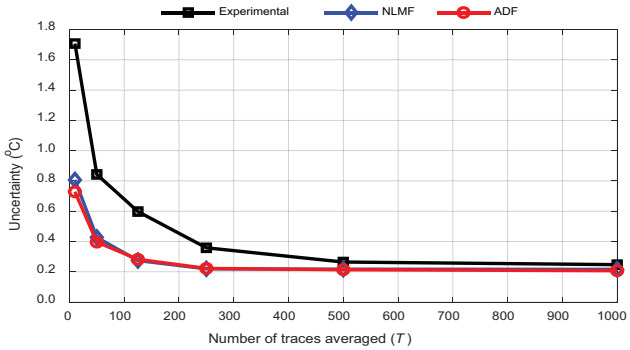

Fig. 6. The uncertainties in temperature extraction from experimental and denoised BGSs for the furthest 50 m section of the 41 km fiber.

The results in Fig. 6 clearly specify that the uncertainty for using both NLMF and ADF are much better than that for the experimental BGSs. For example, the uncertainty for the experimental BGSs at $T = 10$ is ~1.71°C which has been improved to ~0.81°C and ~0.73°C for using NLMF and ADF, respectively. Consequently, the uncertainties in temperature extraction have been improved by 52.63% and 57.31% for using NLMF and ADF, respectively. It can also be found in Fig. 6 that the uncertainties provided by NLMF and ADF at each T are significantly better than that obtained for the experimental BGSs. The results in Fig. 6 thus confirm the robustness of NLMF and ADF in improving the uncertainty of BOTDA sensors in the measurement of temperature.

Next, the effects of using NLMF and ADF on the experimental spatial resolution of the sensor are presented and analyzed. The improvement of SNRs of experimental BGSs for using denoising filters is attained by smoothing the BGSs which relies on the elimination of high frequency components of noisy BGSs [33]. Consequently, the experimental BGSs can be over-smoothed. This over-smoothing of BGSs along the fiber section where temperature changes swiftly can deteriorate the experimental spatial resolution of BOTDA sensors. To authenticate the spatial resolution of the BOTDA sensor after the utilization of both NLMF and ADF clearly, the temperature distributions within the fiber section from 40.940 km to 40.954 km of Fig. 5 where swift change of temperature occurs from ~21 °C to ~45 °C are shown in Fig. 7.

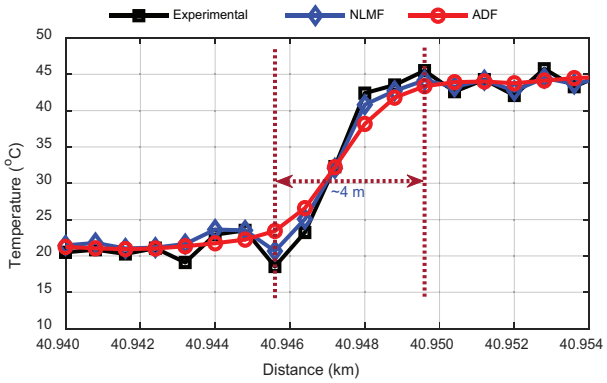

Fig. 7. The verification of the preservation of experimental spatial resolution from the distributions of temperature within the fiber section where temperature changes swiftly.

The temperature distributions in Fig. 7 manifest that both NLMF and ADF can effectively preserve the experimental spatial resolution of 4 m in this study for applying pump pulses having duration of 40 ns in the hardware setup of BOTDA sensor depicted in Fig. 1. The results shown in Fig. 7 again confirm the robustness of NLMF and ADF in preserving the experimental spatial resolution of BOTDA sensors.

The process of determination of temperature distribution from the denoised BGSs requires the denoising of experimental BGSs by applying NLMF or ADF first before applying the process of CFT. This preprocessing stage of denoising of experimental BGSs includes extra runtime to determine the temperature distributions using CFT. However, the processing of denoised BGSs using CFT takes shorter runtime due to the use of less number of iterations as compared to that for using CFT on experimental noisy BGSs [11]. To analyze this, the runtimes in extracting temperature distributions from the experimental and denoised BGSs

are computed and compared. The runtimes are computed for using CFT directly on the experimental BGSs as well as for that on the denoised BGSs obtained after applying NLMF and ADF on the experimental BGSs. Such runtimes are computed separately for the BGSs obtained with six different T in this study. These runtimes are compared in terms of relative runtime T_R. The T_R for using a individual process at a particular T is calculated to be the ratio of runtime for using the process to that for using CFT directly on the experimental BGSs obtained at T = 1000, the largest T (i.e., best SNR) exploited in this study. The outcomes are plotted in Fig. 8.

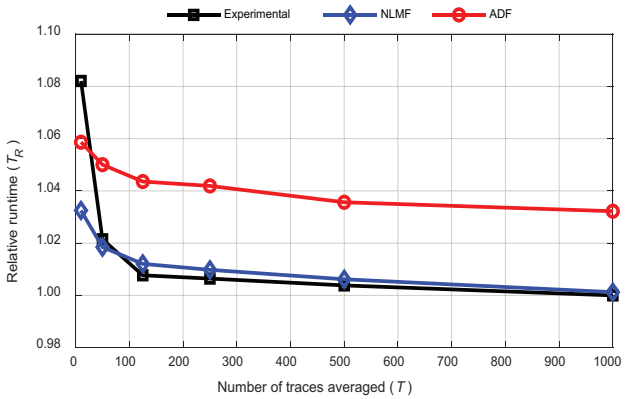

Fig. 8. The variation of relative runtime in extracting temperature distributions from the experimental and denoised BGSs.

It is seen in Fig. 8 that the T_R for applying CFT on the experimental BGSs obtained at T = 10 is the highest, which is due to the fact that the average SNR of the experimental BGSs is also the lowest (i.e., ~8.68 dB) at T = 10 as can be seen in Fig. 4. As a consequence, the process of CFT relatively needs large number of iterations (i.e., longer runtime) to extract temperature distribution from such noisy BGSs. However, after denoising the experimental BGSs obtained at T =10 using NLMF and ADF, the SNRs have been improved to ~22.21 dB and ~24.32 dB, respectively. Consequently, the values of T_R at T = 10 for using CFT on the denoised BGSs having such higher SNRs obtained after applying NLMF and ADF are significantly lower than that for using CFT directly on the experimental BGSs. It is also observed in Fig. 8 that T_R decreases sharply first for increasing T from 10 to 50 and then decreases gradually at a higher T (i.e., higher SNR). This is due to the fact that the utilization of very small T (e.g., T = 10) during the acquisition of BGSs cannot improve the SNRs of the experimental BGSs significantly as compared to that at higher T. This is because the average SNR of the experimental BGSs follows a square root dependency on T [10]. It is remarkably noticed in Fig. 8 that the values of T_R for using CFT on the denoised BGSs obtained after applying NLMF are comparable to that for using CFT on the experimental BGSs obtained at T = 50 to T = 1000. These results indicate that the additional runtime required to denoise the experimental BGSs by applying NLNF in the preprocessing stage is almost balanced by the reduced runtime required in the determination of temperature distributions from the denoised BGSs by applying CFT. However, the determination of temperature distributions using CFT from the denoised BGSs obtained after applying ADF requires only ~3.2% more T_R as compared to that obtained after applying NLMF irrespective of T. In essence, NLMF can be consider as more robust signal denoising technique in term of relative runtime, especially when BGSs are obtained from BOTDA experiment by averaging lower numbers of traces.

6. Conclusions

In this paper, an explicit investigation on denoising of BGSs along a 41 km fiber using NLMF and ADF is demonstrated experimentally. The BGSs are obtained from the experimental setup of BOTDA sensor with different numbers of traces averaged during the acquisition of BGSs. The denoising performances of NLMF and ADF are presented and evaluated systematically in terms of SNR improvement, uncertainty in temperature extraction, spatial resolution and runtime in processing BGSs. The results disclose that the processing of experimental BGSs with the used filters provides BGSs with much higher SNR. As a result, the use of these filters can offer much lower uncertainties in temperature extraction as compared to that without applying such filters on experimental BGSs. Moreover, both NLMF and ADF can preserve the experimental spatial resolution of the BOTDA sensor, which is 4 m in this study. Although the process of denoising of BGSs using NLMF is slightly faster than that using ADF, both of these two filters do not add significant time to denoise the experimental BGSs before the extraction of temperature distributions using CFT. Therefore, both NLMF and ADF can be attractive tools of robust signal denoising for highly accurate and spatial resolution preserved BOTDA sensors. Future study will explore the effectiveness of time-frequency analysis and machine learning based signal processing for high-performance BOTDA sensors.

Acknowledgement

The author thanks University of Dhaka, Dhaka-1000, Bangladesh for the financial support of this work under the Centennial Research Grant (CRG). The data used in this research work have been obtained from the 'Photonics Research Institute' at The Hong Kong Polytechnic University, Hong Kong SAR.

References

1. A. Coscetta, A. Minardo, and L. Zeni, "Distributed Dynamic Strain Sensing Based on Brillouin Scattering in Optical Fibers," *Sensors* 5629, 20(19), pp 1-23, 2020.
2. P. Lu, N. Lalam, M. Badar, B. Liu, B. T. Chorpening, M. P. Buric, and P. R. Ohodnicki, "Distributed optical fiber sensing: Review and perspective," *Appl. Phys. Rev,* 6, pp 1-35, 2019.
3. J. Li, X. Zhou, Y. Xu, L. Qiao, J. Zhang, and M. Zhang, "Slope-assisted Raman distributed optical fiber sensing," *Photon. Res.*, 10(1), pp 205-213, 2022.

4. N. Lalam, P. S. Westbrook, J. Li, P. Lu, and M. P. Buric, "Phase-Sensitive Optical Time Domain Reflectometry With Rayleigh Enhanced Optical Fiber," *IEEE Access*, 9(1), pp 114428-114434, 2021.
5. A. K. Azad, F. N. Khan, W. H. Alarashi, N. Guo, A. P. T. Lau and C. Lu, "Temperature extraction in Brillouin optical time-domain analysis sensors using principal component analysis based pattern recognition," *Opt. Express*, 25(14), pp 16534-16549, 2017.
6. Q. Zhang, T. Wand, J. Zhao, J. Liu, Y. Wang, J. Zhang, L. Qiao, and M. Zhang, " A Dual-Adaptive Denoising Algorithm for Brillouin Optical Time Domain Analysis Sensor," *IEEE Sensors Journal*, 21(20), pp 22712-22719, 2021.
7. X. Angulo-Vinuesa, S. Martin-Lopez, P. Corredera, and M. Gonz´alez-Herr´aez, "Raman-assisted Brillouin optical time-domain analysis with sub-meter resolution over 100 km," *Opt. Express*, 20(11), pp 12147-12154, 2012.
8. S. Wang, Z. Yang, S. Zaslawski, and L. Thévenaz, "Short spatial resolution retrieval from a long pulse Brillouin optical time-domain analysis trace," *Opt. Lett.*, 45(15), pp 4152-4155, 2020.
9. N. D. Nordin, M. S. D. Zan, and F. Abdullah, "Comparative Analysis of the Deployment of Machine Learning Algorithms in the Distributed Brillouin Optical Time Domain Analysis (BOTDA) Fiber Sensor," *Photonics 79*, 7(4), pp 1-13, 2020.
10. M. A. Soto, and L. Thévenaz, "Modeling and evaluating the performance of Brillouin distributed optical fiber sensors," *Opt. Express*, 21(25), pp 31347-31366, 2013.
11. A. Dominguez-Lopez, A. Lopez-Gil, S. Martin-Lopez, M. Gonzalez-Herraez, "Signal-to-Noise Ratio Improvement in BOTDA Using Balanced Detection," *IEEE Photon. Technol. Lett.*, 26(4), pp 338 - 341, 2013.
12. M. A. Farahani, E. Castillo-Guerra, and B. G. Colpitts, "Accurate Estimation of Brillouin frequency shift in Brillouin optical time domain analysis sensors using cross correlation," *Opt. Lett.*, 36(21), pp 4275-4277, 2011.
13. H. Iribas, A. Loayssa, F. Sauser, M. Llera, and S. L. Floch, "Cyclic coding for Brillouin Optical Time-Domain Analyzer using probe dithering," *Opt. Express*, 25(8), pp 8787-8800, 2017.
14. C. Zhao, M. Tang, R. Liao, H. Wu, and S. Fu, "SNR-Enhanced Fast BOTDA Combining Channel Estimation Technique with Complementary Pulse Coding," *IEEE Photonics. J*., 10(5), pp 1-10, 2018.
15. X. Jia, and Y. Rao, L. Chang, C. Zhang and Z. Ran, "Enhanced sensing performance in long distance Brillouin optical time-domain analyzer based on Raman amplification: Theoretical and experimental investigation," *J. Lightwave Technol.* 28(11), pp 1624–1630, 2010.
16. M. A. Soto, X. Angulo-Vinuesa, S. Martin-Lopez, S. Chin, J. D. Ania-Casta˜non, P. Corredera, E. Rochat, M. Gonzalez-Herraez, and L. Th´evenaz, "Extending the real remoteness of long-range Brillouin optical time-domain fiber analyzers," *J. Lightwave Technol.* 32(1), pp 152–162, 2014.
17. M. A. Soto, M. Taki, G. Bolognini, and F. D. Pasquale, "Simplex-coded BOTDA sensors over 120 km SMF with 1-m spatial resolution assisted by optimized bidirectional Raman amplification," EEE *Photon. Tech. Lett.* 24(20), pp 1823-1826, 2012.
18. M. A. Soto, J. A. Ramírez, and L. Thévenaz, "Intensifying the response of distributed optical fibre sensors using 2D and 3D image restoration," *Nat. Commun.* 7:10870, 2016.
19. A. K. Azad, "Analysis of 2D Discrete Wavelet Transform Based Signal Denoising Technique in Brillouin Optical Time Domain Analysis Sensors," *The Dhaka University JASE*, 5(1&2), pp 1-8, 2020.
20. M. A. Farahani, M. T. V. Wylie, E. Castillo-Guerra, and F. G. Colpitts, "Reduction in the number of averages required in BOTDA sensors using wavelet denoising techniques," *J. Lightwave Technol*., 30(8), pp 1134–1142, 2012.
21. A. K. Azad, "Extraction of Temperature Distributions in Brillouin Optical Time Domain Analysis Sensors Using 2D Wiener Filter Based Matched Filter Detection," *The Dhaka University JASE*, 6(2), pp 30-38, 2021.
22. P. Zhang, B. Wang, Y. Yang, A. K. Azad, K. Luo, K. Yu, C. Yu, and C. Lu, "SNR enhancement for Brillouin distributed optical fiber sensors based on asynchronous control," *Opt. Express,* 30(3), pp 4231-4248, 2022.
23. K. Luo, B. Wang, N. Guo, K. Yu, C. Yu, and C. Lu, "Enhancing SNR by Anisotropic Diffusion for Brillouin Distributed Optical Fiber Sensors," *J. Lightwave Technol.*, 38(20), pp 5844-5852, 2020.
24. B. Wang, L. Wang, C. Yu, and C. Lu, " Long-distance BOTDA sensing systems using video-BM3D denoising for both static and slowly varying environment," *Opt. Express*, 27(25), 36100-36113, 2019.
25. X. Qian, X. Jia, Z. Wang, B. Zhang, N. Xue, W. Sun, Q. He, and H. Wu, "Noise level estimation of BOTDA for optimal non-local means denoising," *Appl. Optics*, 56(16), pp 4727-4734, 2017.
26. B. K., S. Kumar, "Image denoising based on non-local means filter and its method noise thresholding," *Signal, Image and Video Processing*, 7(1), pp 1211-1227, (2013).
27. K.M. Prabusankarlal, R. Manavalan, and R. Sivaranjani, "An optimized non-local means filter using automated clustering based preclassification through gap statistics for speckle reduction in breast ultrasound images," *App. Computing and Informatics*, 14(1), pp 48-54, 2018.
28. P. Perona and J. Malik, "Scale-space and edge detection using anisotropic diffusion," *IEEE Trans. on Pattern Analysis and Machine Intelligence*, 12(7), pp 629-639, 1990.
29. C. Tsiotsios, and M. Petrou, "On the choice of the parameters for anisotropic diffusion in image processing," *Pattern Recognition*, 46(1), pp 1369-1381, 2012.
30. J. Immerkær, "Fast Noise Variance Estimation," *Computer Vision and Image Understanding*, 64(2), pp. 300-302, 1996.
31. J. Hu and Y. P. Luo, "Non-local means algorithm with adaptive patch size and bandwidth," *Optik*, 124(22), pp. 5639-5645, 2013.
32. A. K. Azad, L. Wang, N. Guo, H. Y. Tam and C. Lu, "Signal processing using artificial neural network for BOTDA sensor system," *Opt. Express*, 24(6), pp 6769-6782, 2016.
33. Y. P. Chaudhari, and P. M. Mahajan, "Image denoising of various images using wavelet transform and thresholding techniques," *Int. Research. J. Engg. Technol.* 4(2), pp 517-523, 2017.